

Measurement of functional resilience of transport network

Citation for published version (APA):

Wang, J., Liao, F., Wu, J., Sun, H., Wang, W., & Gao, Z. (2023). Measurement of functional resilience of transport network: The case of the Beijing subway network. *Transport Policy*, 140, 54-67.
<https://doi.org/10.1016/j.tranpol.2023.06.016>

Document license:

CC BY

DOI:

[10.1016/j.tranpol.2023.06.016](https://doi.org/10.1016/j.tranpol.2023.06.016)

Document status and date:

Published: 01/09/2023

Document Version:

Publisher's PDF, also known as Version of Record (includes final page, issue and volume numbers)

Please check the document version of this publication:

- A submitted manuscript is the version of the article upon submission and before peer-review. There can be important differences between the submitted version and the official published version of record. People interested in the research are advised to contact the author for the final version of the publication, or visit the DOI to the publisher's website.
- The final author version and the galley proof are versions of the publication after peer review.
- The final published version features the final layout of the paper including the volume, issue and page numbers.

[Link to publication](#)

General rights

Copyright and moral rights for the publications made accessible in the public portal are retained by the authors and/or other copyright owners and it is a condition of accessing publications that users recognise and abide by the legal requirements associated with these rights.

- Users may download and print one copy of any publication from the public portal for the purpose of private study or research.
- You may not further distribute the material or use it for any profit-making activity or commercial gain
- You may freely distribute the URL identifying the publication in the public portal.

If the publication is distributed under the terms of Article 25fa of the Dutch Copyright Act, indicated by the "Taverne" license above, please follow below link for the End User Agreement:

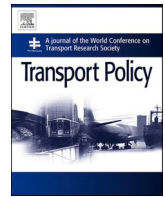
www.tue.nl/taverne

Take down policy

If you believe that this document breaches copyright please contact us at:

openaccess@tue.nl

providing details and we will investigate your claim.



Measurement of functional resilience of transport network: The case of the Beijing subway network

Junjie Wang^{a,b}, Feixiong Liao^{b,*}, Jianjun Wu^{c,**}, Huijun Sun^a, Weiping Wang^a, Ziyou Gao^{a,***}

^a School of Systems Science, Beijing Jiaotong University, Beijing, China

^b Urban Planning and Transportation Group, Eindhoven University of Technology, the Netherlands

^c State Key Laboratory of Advanced Rail Autonomous Operation, Beijing Jiaotong University, China

ARTICLE INFO

Keywords:

Functional resilience
Robustness
Adaptability
Recoverability

ABSTRACT

Resilience is an important concept for measuring a system's ability to cope with various disruptions. This study proposes an application-oriented framework for measuring the dynamic functional resilience (FR) of a transport network responding to supply and demand disruptions without external interventions. On the conceptual side, three complementary capacity-related dimensions, namely, robustness, adaptability, and recoverability, are incorporated in the single FR framework from the perspective of physical laws. On the applied side, we suggest a measurement model given certain network indices and apply it to the Beijing subway network (BSN). The results indicate the measurement model can capture the dynamics of network performances, identify the time-varying bottlenecks, and predict the influence of the dynamic capacity expansions on network resilience. The findings are useful for policy-making regarding the dynamic design, operation, and reconstruction of the transport infrastructure.

1. Introduction

Transport networks play a pivotal role in mobility for the social and economic development of modern cities. However, various disruptions to the nodes or edges of a transport network may affect the network structure, function, and efficiency (Ganin et al., 2017; Wang et al., 2018; Gu et al., 2020). Therefore, operators need to ensure the resilience of transport networks. Resilience has been one of the most used performance measures on all kinds of transport systems (Chen and Miller-Hooks, 2012; Wang et al., 2013; Baroud et al., 2014) under disruptions. The measurement of resilience under various disruptions is instrumental for policy-making toward the design, operation, and reconstruction of transport networks (Ganin et al., 2017).

Resilience has been defined in different ways. Many similar concepts to “resilience” are compared (Bruneau et al., 2003; Murray-Tuite, 2006; Linkov et al., 2015; Kermanshah and Derrible, 2017; Liao and van Wee, 2017; Galaitsi et al., 2020; Qin and Liao, 2021; Wu et al., 2021; Zeng et al., 2021; Zuo, 2021), including robustness, redundancy, resourcefulness, rapidity, diversity, efficiency, autonomous components, strength, collaboration, adaptability, mobility, accessibility, safety,

recovery, absorb, reliability, vulnerability, risk, and sustainability. A few recent reviews (Zhou et al., 2019; Gu et al., 2020; Galaitsi et al., 2021; Serdar et al., 2022) also indicated resilience is a multidimensional concept and there is no consensus on the definition and connotation.

Different definitions of resilience may result in different measurements for quantifying resilience in single or multiple dimensions. To better compare the differences and similarities between resilience dimensions, a few researchers clarified the related concepts from different perspectives. Based on the performance indices used in the measurement, Gu et al. (2020) made a distinction between three related terms, including reliability, vulnerability, and resilience. They summarized four types of performance indices: travel time, connectivity, accessibility, and capacity. Galaitsi et al. (2020, 2021) compared a number of related concepts (e.g., risk, reliability, robustness, vulnerability, sustainability, safety) facing threats from disruptions, linguistic characteristics, and system responses. Although they offered valuable insights into the definitions and quantifications of resilience, there are two limitations. First, the definitions and connotations of resilience have overlaps with other concepts. Second, the definitions of resilience are general but not specific in the context of transport networks.

* Corresponding author.

** Corresponding author.

*** Corresponding author.

E-mail addresses: f.liao@tue.nl (F. Liao), jjwu1@bjtu.edu.cn (J. Wu), zygao@bjtu.edu.cn (Z. Gao).

<https://doi.org/10.1016/j.tranpol.2023.06.016>

Received 22 August 2022; Received in revised form 9 April 2023; Accepted 30 June 2023

Available online 3 July 2023

0967-070X/© 2023 The Author(s). Published by Elsevier Ltd. This is an open access article under the CC BY license (<http://creativecommons.org/licenses/by/4.0/>).

In transport networks, the demand and supply may vary over time and they both lead to dynamic system performances. After the disruptions, the passengers would spontaneously perform rerouting in the transport networks, which may propagate the disruptions (Motter and Lai, 2002; Zhang et al., 2019) and cause cascading failures to the networks.

In response to the disruptions and cascading failures, the transport network operators are concerned with the functionality of the networks. We use “function” to refer to the circumstance that the transport network remains functional after supply and demand disruptions (Kitsak et al., 2018). Accordingly, we propose an application-oriented framework of “functional resilience (FR)” to describe and measure the dynamic FR of transport networks without external interventions under supply and demand disruptions. The necessary components of the framework include resilience dimensions, dynamic travel demand and network supply interactions, demand and supply disruptions, and targeted network indices. We compare the element differences between our framework and some relevant ones in Table 1. First of all, as shown, most studies only considered single resilience dimensions and those few with multiple dimensions have the limitations summarized above. We select three different but complementary dimensions. Second, for the disruption types, Galatsi et al. (2020) proposed chronic and acute disruption types, and furtherly Sedar et al. (2022) divided them into natural hazards, intentional attacks, accidents, and failure propagations. Since few have taken into account surging travel demands as disruptions, the supply side as well as the demand side are considered in our framework. Third, while various targeted indices are separately used for different dimensions (e.g., Gu et al., 2020; Sedar et al., 2022), all the targeted indices can be encapsulated into our framework and compared cross dimensions. Fourth, for modeling the demand and supply interactions, a cascading failure model (Motter and Lai, 2002) is employed in this study to simulate the subsequent failures on the network after the initial supply disruptions, which has seldom been considered in the existing studies. Therefore, the proposed framework has the advantages of complementary resilience dimensions, comprehensive targeted indices, the integration of cascading failures into the demand and supply interactions, and the consideration of demand disruptions.

The study makes contributions from the conceptual and applied points of view. For the conceptual contribution, three capacity-related dimensions are extracted from the literature. They are conceptualized holistically with physical interpretations, which are easy to understand and avoid the overlaps that commonly appear in the past definitions of resilience. For applying the measurement model, we entail with high integrity the comprehensive resilience dimensions, dynamic travel demand and network supply interactions, demand and supply disruptions, and targeted network indices. In the case study of the Beijing subway

network (BSN), the results indicate the proposed framework can capture the dynamics of network performances, pinpoint the time-varying bottlenecks, and predict the influence of the dynamic capacity expansions on network resilience. The findings are useful for policy-making regarding the dynamic design, operation, and reconstruction of transport networks.

The remainder of this paper is organized as follows. Section 2 presents the conceptualization of the FR. Section 3 presents the measurement framework and operationalization of FR. In Section 4, a case study using the BSN is carried out to verify the measurement framework. Section 5 discusses the measures to improve resilience and gives some policy suggestions. Section 6 summarizes the contributions of this paper and discusses the prospects for future work.

2. Conceptualization of FR of transport network

This section formally discusses the concept of FR in the context of a transport network. To facilitate the understanding of the essential ideas, we introduce the transport network setting and explain the chosen measuring dimensions of FR.

2.1. Setting

A typical transport network $G(V, E)$ encompasses the following components: a set of nodes (V) and edges (E), the carrying capacities of the nodes (C_v) and edges (C_E), and the traffic volume through the nodes (q_v) and edges (q_E) of a timeslot of interest. The carrying capacities are usually imposed by the supply side and thus may be changing at different periods. Travel demand may be dynamic in different timeslots of the entire time frame but is considered relatively stable in the same timeslot of different time frames. One time frame starts at the time point when a disruption happens and, possibly after multiple disruptions, ends at the time point when the disruption(s) would no longer affect stability. The time frame is divided into K ($K \in \mathbb{N}^+$) timeslots to capture the dynamicity of the travel demand and the different impacts on the transport network. In that sense, the total travel demand (D^k ; $k \in [1, K]$) in the k -th timeslot can be divided into two parts, the stable travel demand (D_s^k) and the extra travel demand (D_c^k), to represent stability and dynamicity, respectively. Similarly, the volume of the stable travel demand from node i to node j ($D_s^k(i, j)$, $i, j \in V, i \neq j$) is quasi-dynamic. Unless otherwise stated, the notations (see Table A1 in Appendix 1) with elements bracketed refer to scalar values (e.g., $D_s^k(i, j)$) and those without are vectors (e.g., D_s^k).

It is supposed that after the disruption, the network can reach another stable state during each timeslot. The maximum impact cannot be reached at the same moment of disruption, which is reasonable due to

Table 1
The element comparisons between the proposed framework and others.

| Reference | Dimensions | Disruption type | Targeted indices | Cascading failures |
|----------------------------------|---|--|---|--------------------|
| Henry and Ramirez-Marquez (2012) | recovery | supply side | time, cost, and speed | no |
| He and Liu (2012) | remainder | supply side | link flow | yes |
| Espinet et al. (2016) | vulnerability | climate change | fiscal cost, kilometer damage, and opportunity cost | no |
| Nogal et al. (2016) | recovery | supply side | cost, impedance, and user stress level | no |
| Nogal and Honfi (2019) | recovery | supply side | link flow ratio | no |
| Wang et al. (2019) | recovery | water flood | connectivity | no |
| Zhou et al. (2019) | four dimensions from maintenance and recovery aspects | supply side | performance, topological, and attribute-based | no |
| Gu et al. (2020) | resistance and recovery | supply side | connectivity and efficiency | no |
| Li et al. (2020) | robustness | extreme environment | mobility and connectivity | no |
| Sedar et al. (2022) | seven different dimensions with overlaps | natural hazards, intentional attacks, accidents, and failure propagation | performance, connectivity, cost, statistic, and qualitative | no |
| This study | three different but complementary dimensions | demand and supply sides | all indices can be embedded | yes |

the continuity and the nature of lagged traffic propagation. As the real network performance during timeslot k may be unstable or even unknown, the results at the new equilibrium state are selected for reference purposes. The FR is jointly affected by the targeted network index (x), the stable travel demand in the k -th timeslot (D_s^k), and the disruption d . The disruption d can be from the supply side, demand side, or both occurring in different timeslots. The FR dimensions may also be dynamic with respect to t . A general expression of FR is written as $\mathcal{R}(x, D_s^k, d, t)$. To better capture a transport network's responses to disruption, we discern the difference between structural resilience (SR) and FR. The main difference between SR and FR resides in the dynamic demand-supply interactions that occur on the network (Motter and Lai, 2002; Holme et al., 2002; Gu et al., 2020).

2.2. Three capacity-based dimensions of FR

Researchers (Bruneau et al., 2003; Zhou et al., 2019; Gu et al., 2020) compared the concepts of resistance, vulnerability, and robustness. It is not hard to find that robustness is an inverse concept of vulnerability but a similar one of resistance. Thus, the selection of any one of these three is representative to measure the capacity surplus or loss of a network, implying that the other two are redundant. Note that the term capacity refers to network performance in a broad sense and is indicated by a specific index in the operationalization. In addition, by comparing the recoverability addressed by Zhang et al. (2019) and robustness by Zeng et al. (2019), we find robustness is a transient value of the network performance, but recoverability is the accumulation of the transient values during the recovery process. In other words, there are strong correlations among the resilience dimensions aforementioned. To reduce the resilience dimensions, we set aside the literal differences between the concepts and focus on the actual measurement differences. Various keywords of 25 resilience-related studies are compared and summarized in Table A2 (see Appendix 1). They can be categorized into three dimensions. Since existing studies are mixed in using the concepts to describe different dimensions, we place the concept(s) from each study in the corresponding column(s) in terms of the matching connotation(s). For the first dimension, resistance (Zhang et al., 2015), robustness (Bruneau et al., 2003; Zeng et al., 2019), vulnerability (Wang et al., 2013; Reggiani et al., 2015; Gu et al., 2020), connectivity (Murray-Tuite, 2006), etc. concern the capacity surplus and these concepts are placed in the first column. For the second dimension, adaptability (Murray-Tuite 2006), absorb (Zhang et al., 2015), etc. focus on the capacity change and they are placed in the second column. For the third dimension, recovery (Chen and Miller-Hooks, 2012; Gu et al., 2020), recoverability (Zhang et al., 2019), rapidity (Bruneau et al., 2003), etc. capture the cumulative capacity loss and they are placed in the third column. Thus, resilience can be decomposed into three dimensions: robustness, adaptability, and recoverability. As summarized in Table A2, they represent the transport network's capacity surplus, change, and cumulative loss after disruptions.

2.3. Interpretations and formulations

To elaborate on the relationships among the three dimensions, the entities and specific definitions of them are described in transport network G as follows. Robustness is to measure the capacity surplus compared to its original state after disruption d happens; adaptability is to measure the capacity change used to adapt to d compared to its former state; recoverability is to measure the cumulative capacity loss to recover from d during a time frame. The three dimensions can be interpreted with a metaphor in physics shown in Fig. 1. In the k -th timeslot, the ball receives forces in three cases (Fig. 1a). First, when it is placed on the ground statically as the initial stable state 1 (in analogy to an equilibrium state in a transport network) at t_b^k , its gravity (in analogy to D_s^k) is applied to the ball and the shape may slightly change. When it is lifted into the air and the support force from the ground is gone, the shape reaches its full size. If we pat the ball with a certain strength (in analogy to D_s^k and d) onto the ground, the shape may change significantly at the time when the ball hits the ground. Quantifying the transient capacity surplus during timeslot k , denoted by the area of R_1 , is the first dimension of resilience, i.e., robustness. Second, in the meantime, quantifying the transient deformation, denoted by the area of R_2 , to adapt to the patting strength refers to the second dimension of resilience, i.e., adaptability. Given the maximum deformation at t_w^k , the ball has the worst robustness and adaptability. Finally, quantifying the entire continuous deformation process until the ball recovers to stable state 2 at t_f^k corresponds to the third dimension of resilience, i.e., recoverability. Note that the ball area under the ground in stable state 1 may not be the same as that in 2 because the disruption may cause irreversible change to the ball during the entire recovery process. While for SR, the ball would not recover after it hits the ground until it is repaired by external forces, meaning that the shape-changing is constant.

The physical relationships among them can be further interpreted by three performance curves in Fig. 1 (b). The x-axis stands for the progress of time t and the y-axis stands for the network's transient performance at time point t . Suppose that in addition to any possible disruptions before timeslot k , disruption d happens at t_b^k with the greatest impact on the network performance at t_w^k and a new stable state is achieved at t_f^k . Several studies (Bruneau et al., 2003; Gu et al., 2020) stipulated that the robustness of a system is measured only at t_w^k and the recovery process also starts at t_w^k . However, the impact of the disruption on the network is constantly changing and the recovery actually exists during the entire time frame. At each time point of timeslot k , robustness and adaptability can be measured and they represent a system's variable performances and the recovery process involves the entire time frame. The dashed horizontal line $\mathcal{R}(0)$ represents the network resilience when there is neither D_s^k nor d ; the blue curve $\mathcal{R}(D_s^k)$ represents the network resilience only with D_s^k ; and the red curve $\mathcal{R}(D_s^k, d)$ represents the network resilience with both D_s^k and d . The height of $\mathcal{R}(D_s^k, d)$ with reference to the

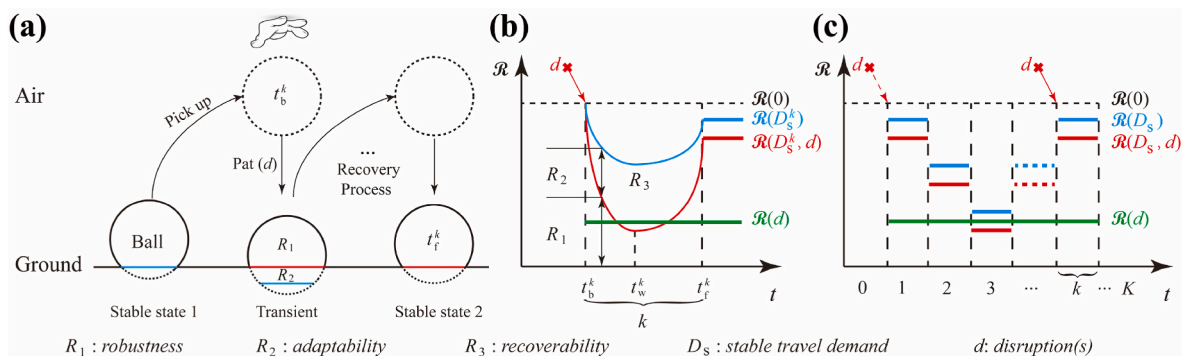


Fig. 1. Conceptualization of the three dimensions of FR.

x-axis represents the transient network robustness at t ; the height difference between $\mathcal{R}(D_s^k, d)$ and $\mathcal{R}(D_s^k)$ is the transient network adaptability at t ; the area between $\mathcal{R}(0)$ and $\mathcal{R}(D_s^k, d)$ is the network recoverability during a timeslot related to d . In case of irreversible change (permanent damage) to the ball by a strong patting force, the height difference (potentially large) between the blue line and the red line after t_b^k represents the permanent capacity loss.

Fig. 1 (b) shows SR indicated by the green line is static but FR describes a dynamic process. Fig. 1 (c) shows the difference between SR and FR in the entire time frame of K timeslots on condition that the targeted network indices are the same. For the sake of simplicity, Fig. 1 (c) only illustrates the network performances at the final equilibrium states in different timeslots. While the thick green line represents the fixed SR, the thicker blue lines (without d) and red lines (with d) together form the FR. As there are no traffic dynamics in the measurement of SR, SR only depends on disruption. However, FR depends both on disruption and D_s^k , and the latter is time-dependent with respect to timeslot k .

The measurements of the three dimensions of FR are formulated as follows.

2.3.1. Robustness

Robustness (denoted by R_1) is to measure G 's capacity surplus under D_s^k and d during timeslot k . With targeted network index x , the general expression of robustness at time point t is written as Eq. (1). The larger R_1 is, the more capacity surplus the network has and the more resilient it is.

$$R_1 = \mathcal{R}(x, D_s^k, d, t), k \in [1, K] \quad (1)$$

2.3.2. Adaptability

Adaptability (denoted by R_2) is to measure G 's changing capacity to adapt to disruption d under D_s^k during timeslot k . With the same x , the general expression of adaptability is written as Eq. (2). As shown in Fig. 1 (b), $\mathcal{R}(x, D_s^k, 0, t)$ stands for the network performance only with D_s^k at stable state 1, where $d = 0$ means no disruption. The smaller R_2 is, the stronger adaptability the network has to the disruption and the more resilient it is.

$$R_2 = \mathcal{R}(x, D_s^k, 0, t) - \mathcal{R}(x, D_s^k, d, t), k \in [1, K] \quad (2)$$

2.3.3. Recoverability

Recoverability (denoted by R_3) is to measure G 's cumulative capacity loss from disruption d under D_s^k during the time frame between t_b^k and t_f^k . Compared to Zhang et al. (2019) who used a shaded triangle area to measure a network's resilience, we use a generalized form, Eq. (3), to measure the recoverability of FR. The smaller R_3 is, the smaller effects the disruption causes to the network, standing for higher recoverability.

$$R_3 = \int_{t_b^k}^{t_f^k} [\mathcal{R}(x, 0, 0, t) - \mathcal{R}(x, D_s^k, d, t)] dt, k \in [1, K] \quad (3)$$

One may argue that the benchmark network performance in Eq. (2) seems to be associated with D_s^k and the dimension of adaptability can be reduced to Eq. (1). In fact, the benchmark is $\mathcal{R}(x, 0, 0, t)$ in Eqs. (1) and (3), which stands for the maximum network performance under free-flow conditions. The adaptability aims to quantify the capacity change due to the disruptions, but D_s^k may also decrease the network capacity, which is not attributed to the disruption (Ganin et al., 2017; Zhang et al., 2019). Therefore, the second dimension of adaptability is not redundant. Also note that when the length of timeslot k approaches zero, it appears that FR can capture the real-time dynamic process on the network. However, the network may not reach a new equilibrium state at the end of the timeslot of interest, which causes incapability of measuring the recoverability dimension. Therefore, the length of timeslot k is set long

enough for the network to reach equilibrium after the disruption. With this consideration, the results at the new equilibrium state are preferably used as the resilient performance, although the measurements of FR are formulated in fully dynamic forms. It should also be noted that if $D_s^k = 0$ and time t is removed in Eqs. (1)–(3), the generalized formulations of FR degenerate into those of SR.

3. Operationalization

This section presents a measurement framework for operationalization in the context of trip-based travel demand analysis. The framework consists of network configuration, traffic dynamics, disruption, the new equilibrium state, and three FR dimensions according to the targeted index.

The framework is depicted in Fig. 2. First, $G(V, E)$ is constructed based on the spatial structure and the static and dynamic attributes of the nodes and edges. Second, given the travel demand in different timeslots of an average day, traffic dynamics on the network take place in the presence of direct and indirect disruption. According to the traditional four-step models, this module includes trip generation, trip distribution, modal split, and traffic assignment. In response to disruption, the congestion effects or failure rules are applied to the traffic assignment. The disruption effects are not considered in the first three steps. Traffic assignment is to determine the network flow patterns with regard to travel demand and network supply interactions. The network may be congested or even blocked to lose functions. To simulate the cascading failures, we employ the failure model suggested by Motter and Lai (2002) as follows. The nodes or edges are considered failures and removed when $b_d > (1 + \alpha)b_{\bar{d}}$, where b_d and $b_{\bar{d}}$ are the node or edge traffic flow and capacity after and before disruption and α refers to a ratio of the network's design capacity that can be used as reserve capacity after the disruptions. After the first assignment, the failures will

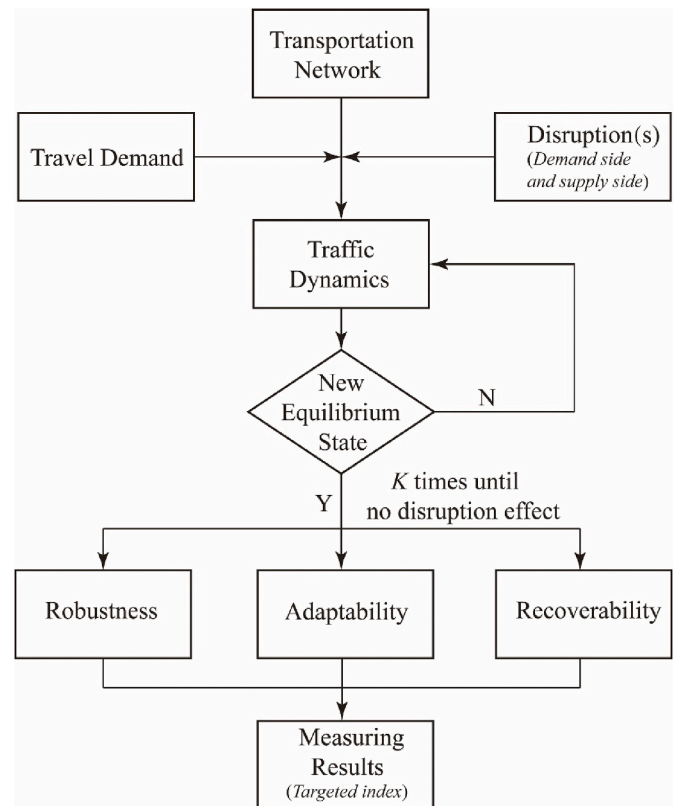


Fig. 2. Measurement framework of FR.

be assessed and removed. The failure rules act on the traffic dynamics until no failure occurs and the network reaches a new equilibrium state. In the traffic assignment, the impedance between each O-D pair is the key factor. For road networks, it is easy to use the BPR equation (U.S. Bureau of Public Roads, 1964) to calculate the impedance; for public transit networks, the impedance consists of waiting time at the starting station, in-vehicle time, and transfer time at the transfer station (Liu et al., 2016). The waiting time and transfer time are assumed to be constant. Passengers choose their routes according to the congestion level in the vehicle as it affects passengers' comfort and the perceived in-vehicle time. Thus, the edge impedances in the road network and public transit network are formulated as Eqs. (4) and (5) respectively

$$t_1(u) = t_0(u) \left[1 + \theta_1 \left(\frac{q_{E_1}(u)}{C_{E_1}(u)} \right)^{\beta_1} \right], u \in E_1 \quad (4)$$

$$t_1(u) = t_0(u) \left[1 + \theta_2 \left(\frac{\max \{q_{E_2}(u) - \rho C_{E_2}(u), 0\}}{C_{E_2}(u)} \right)^{\beta_2} \right], u \in E_2 \quad (5)$$

where $t_0(u)$ is the free-flow travel time of edge u and $t_1(u)$ is the actual or perceived travel time to get through edge u ; $\theta_1, \theta_2, \beta_1$, and β_2 are parameters of the standard BPR equation and the extended form; ρ ($\rho \in [0, 1]$) is a scaling coefficient of the capacity; $q_{E_1}(u)$ and $q_{E_2}(u)$ are the traffic flow of edge u ; $C_{E_1}(u)$ and $C_{E_2}(u)$ is the carrying capacity of edge u .

The Wardrop's first principle for user equilibrium (Wardrop, 1952) is applied as the mechanism for traffic assignment. After the network reaches a new equilibrium state in each timeslot, the measurements are performed on the differences between the previous and the new states for robustness and adaptability. While for recoverability, the measurement result is the accumulation from the initial timeslot to the timeslot K when the disruption no longer affects the network. Based on the same index, all the dimensions of resilience are measured and compared in the framework.

The disruptions are classified into supply disruptions (e.g., accidents or intentional shut-down); and demand disruptions (e.g., extra travel demand). The second type is more common in reality and the extra travel demand D_c^k can be described in three scenarios. D_c^k occurs to a certain node in the first two scenarios (S1 and S2) and to the entire network in the third scenario (S3).

- (1) S1: suppose an emergency event occurs at origin i , which causes an extra fixed volume of demand M during timeslot k . M is proportionally allocated to all destinations that are associated with i .
- (2) S2: due to an emergency event at origin i , each OD pair $i \rightarrow j, \forall j \in V, j \neq i$, has an increased travel demand by a common factor r_0 .
- (3) S3: suppose a disruption occurs to G , every OD pair $i \rightarrow j, \forall i, j \in V, i \neq j$, has an increased travel demand by a common factor r_1 .

Based on the scenario setups, the total and extra travel demand are formulated as Eqs. (6)–(7)

$$D^k(i, j) = D_s^k(i, j) + D_c^k(i, j), \forall i, j \in V, i \neq j \quad (6)$$

$$D_c^k(i, j) = \begin{cases} \frac{M \bullet D_s^k(i, j)}{\sum_{j \in V, j \neq i} D_s^k(i, j)}, i \in V, \forall j \in V, j \neq i & \text{if S1} \\ r_0 \bullet D_s^k(i, j), i \in V, \forall j \in V, j \neq i & \text{if S2} \\ r_1 \bullet D_s^k(i, j), \forall i, j \in V, i \neq j & \text{if S3} \end{cases} \quad (7)$$

where $D^k(i, j)$, $D_s^k(i, j)$ and $D_c^k(i, j)$ are the total, stable, and extra travel demands of OD pair $i \rightarrow j$ during timeslot k , respectively.

The above framework encloses the general modules and necessary components to measure a transport network's FR. The operationalization is applicable for the resilience analysis at the strategic and tactical

levels due to the applications of classic mechanisms for travel demand, network equilibrium, and disruption. The framework can also be extended with the replacement of higher realism counterparts (He and Liu, 2012; Nogal et al., 2016) that better capture the dynamics.

4. A case study of FR measurement: the BSN

This section carries out numerical experiments to demonstrate the measurement of FR using the BSN. First, we describe the characteristics of the datasets and preliminary analysis of the network structure. Then, we present the results of the three dimensions of FR.

4.1. Datasets description

The used datasets include the BSN structure and real travel demand data. The preliminary analyses of these datasets show the time-varying travel demand patterns and the limitations of SR in the resilience measurement (see Appendix 2).

The directed and weighted BSN consists of 268 stations and 603 sections between two neighboring stations. Network attributes were collected from the official website of the Beijing Subway operator. Sectional capacities and running times (including dwelling times at stations) were collected. Each section's carrying capacity $C_{E_2}(u)$ is calculated according to a simplified capacity method for the railway lines (UIC, 2004) as Eq. (8):

$$C_{E_2}(u) = \frac{\Delta t}{t_h} \lambda n_c, u \in E_2 \quad (8)$$

where $C_{E_2}(u)$ is the carrying capacity of section (edge) u ; Δt is a timeslot with 1 h in length; t_h is the headway of a subway line; λ is the rated carrying capacity per carriage; n_c is the number of carriages of a train. The sectional capacities of the BSN are dynamic with t_h , which includes three different operation modes on a day.

The dynamic travel demand was generated using four consecutive weeks of smart card data of the Beijing Subway in August 2015, including the station-to-station check-in and check-out aggregate information. During each time frame k , the travel demands are assigned to the BSN by the method of successive averages (MSA) (Poon et al., 2004). After the initial assignment of the travel demand by the all-or-nothing method, we obtain the initial traffic flow $F(I)$, $I = 1$. Then the augmented traffic flow $Y(I)$ can be calculated according to the former travel cost. The traffic flow $F(I+1)$ is updated by $F(I+1) = F(I) + \frac{1}{I} * (Y(I) - F(I))$ until the two neighboring traffic flows are close enough ($\sum \text{fabs}(F(I+1) - F(I)) \leq 0.001$) or the iteration count reaches a threshold (e.g., $I \geq 50$). Thereafter, the first equilibrium flow is obtained. After the first assignment, the cascading failures will be assessed and removed. Then, we reassign the total travel demand to the disrupted network and assess the failures until no failure occurs. Finally, the new equilibrium state is reached.

4.2. FR of the BSN

The FR of the BSN is measured in the three dimensions respectively. A series of experiments are done based on the general form of resilience measurement $\mathcal{R}(x, D_s^k, d, t)$.

The general experiment settings are as follows. One representative index g (Motter and Lai, 2002; Wang et al., 2018; Yosef et al., 2018; Kitsak et al., 2018; Zhang et al., 2019) commonly used to measure network resilience is adopted in the measurements. After disruption, temporal disconnection or overload situations can occur to the network and it may fall apart into subgraphs. g is the ratio of the maximum connecting subgraph, formulated as

$$g = \frac{n_{G_m}}{n_G} \quad (9)$$

where n_{G_m} is the edge or node number of the maximum connecting subgraph G_m after disruption; n_G is the total number of edges or nodes in the original network G . Timeslot k is set as an hour. D_s^k is the stable travel demand in the k -th hour ($k \in [5, 23]$) of an ordinary day. We focus on a timeslot during the peak hours for measuring robustness and adaptability, while an average operating day for recoverability to study the effects of intense traffic flows. From the preliminary analysis, the extra traffic is observed with the highest fluctuation of 10,000 trips per hour over the stable travel demand. Three different scenarios are defined: S1 ($M = 10,000$), S2 ($r_0 = 1.0$), and S3 ($r_1 = 0 - 0.1$) according to Eqs. (6) and (7). Among them, S1 and S2 refer to the demand disruption that occurs to a station one by one, and S3 refers to the disruption that occurs to all the stations. The experiment settings are in the same form of $\mathcal{R}(g, D_s^k, d)$.

4.2.1. Comparison between SR and FR under supply side disruptions

First, the comparison between FR and SR is conducted based on the same supply disruptions. In Fig. 3 (a), the green, brown, and yellow curves are the robustness curves. They suffer the same supply disruptions (d_{SS}) with the same node failure ratio of r_{SS} and cascading failures are not considered. The three curves are obtained by removing the nodes one by one according to the descending order of the structure-based index of betweenness centrality (green curve), function-based index of traffic flow (yellow curve), or at random (brown curve). The brown curve is depicted with the average result of multiple times of repeated experiments according to Holme et al. (2002). The results show that the “Random” curve is always smaller than the “Structure” and “Function” curves and the “Function” curve is significantly larger than the “Structure” when r_{SS} is around 0.1 but smaller between 0.15 and 0.4. The inconformity of the three network failure modes demonstrates that the real traffic distribution has a low correlation with the structural index.

As cascading failure may cause bigger differences between function-based and structure-based results, two series of experiments are set with $\mathcal{R}(g, D_s^7, d_{SS})$ and $\mathcal{R}(g, D_s^{18}, d_{SS})$ in Fig. 3 (b). In Fig. 3 (b), the supply failures are the same for function-based and structure-based experiments based on the descending order of real traffic volume in the morning peak hour (AM for short) and afternoon peak hour (PM for short). The failure rules for the function-based and structure-based experiments are set as depicted in Section 4.1. Fig. 3 (b) shows the comparison between two dashed SR curves (AM Structure and PM Structure) and two solid FR curves (AM Function and PM Function) considering the effects of α . In the morning peak, the Function curve is below the Structure curve when $\alpha < 0.356$; when $\alpha \geq 0.7$, both AM curves reach 1. In the afternoon peak, the Function curve is always over the Structure curve, and both PM curves reach 1 when $\alpha \geq 0.3$. The following conclusions can be drawn from Fig. 3 (b): (1) comparing AM curves with PM

curves, the robustness differs with the time of day due to the dynamic travel demand; (2) comparing the Function curves with the Structure curves, the dramatic differences in robustness also show that travel demand is a necessary component in the measurement of FR.

The differences among the three curves in Fig. 3 (a) are much smaller than that between the two Function curves in Fig. 3 (b), demonstrating that cascading failure affects robustness dramatically.

4.2.2. Robustness

For the dimension of robustness, the experimental results under different disruption scenarios are compared. We run the series of experiments of $\mathcal{R}(g, D_s^7, d_{D_c^7})$ under scenarios S1 – S3, where $d_{D_c^7}$ refers to the demand disruption of the extra travel demand D_c^7 in the morning peak hour from 7:00 a.m. to 8:00 a.m. The effects of three demand scenarios on robustness are shown in Fig. 4.

First, $\mathcal{R}(g, D_c^7, d_{S1(M=10,000)})$ is set under different values of α from 0 to 0.7 in Fig. 4 (a) with the extra 10,000 trips per hour (M) under S1. Without extra travel demand, all stations should correspond to the values of g on a line in red ($g = 0.1$), brown ($g = 0.12$), yellow ($g = 0.12$), green ($g = 0.12$), cyan ($g = 0.53$), blue ($g = 0.65$), purple ($g = 0.99$), and black ($g = 1.00$). This setup enables us to pinpoint the key stations sensitive to the fixed D_c^7 . In Fig. 4 (a), some stations have values located below the corresponding lines, especially the key stations surrounded by the different colors of ovals, and the larger height difference means greater harm to the network robustness. As shown, the large height differences concentrate within the range of $\alpha \in (0.3, 0.6)$, and S1 has less impact on robustness in the other ranges.

Second, the results of $\mathcal{R}(g, D_c^7, d_{S2(r_0=1.0)})$ under different α can be seen in Fig. 4 (b) with $r_0 = 1.0$ under S2. This setup aims to locate the key stations sensitive to the extra travel demand beyond the stable travel demand. The results show a similar trend as S1 within the range of $\alpha \in (0.3, 0.6)$, but S2 does less harm to the network than S1. It is observed that a smaller number of key stations under S2 have a sharp reaction to extra travel demand and these key stations surrounded by the different colors of ovals are different from S1.

Third, the results of $\mathcal{R}(g, D_c^7, d_{S3(r_1=0-0.1)})$ under different α can be seen in Fig. 4 (c) with different r_1 within $[0.00, 0.10]$ under S3. g presents a ladder-type descending trend with the increase of r_1 and grows sharply with the increase of α . Similarly, when $\alpha > 0.6$, g is over 98%, but if $\alpha \leq 0.3$, g is not affected by r_1 . Within the range (0.3, 0.6), a small r_1 does great harm to the robustness. This implies that with the increase in travel demand, the network may face a severe issue of robustness.

4.2.3. Adaptability

Adaptability measures the capacity change of the BSN resulting from a stable travel demand to three different demand disruptions. The

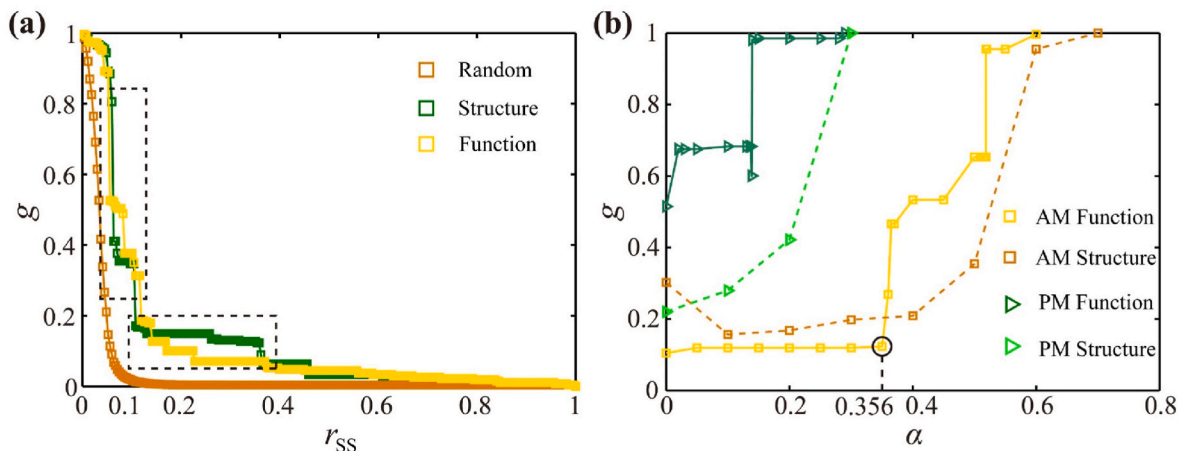


Fig. 3. Robustness comparison of the BSN between SR and FR.

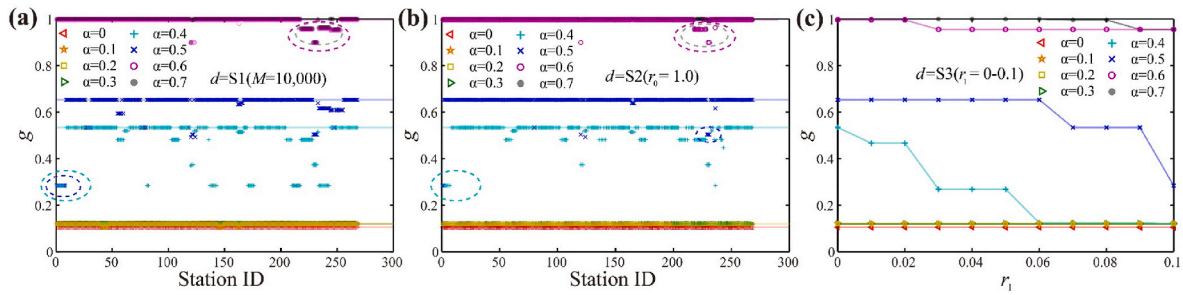


Fig. 4. The robustness of the BSN under S1, S2, and S3.

disruptions and experiment parameters are set the same as those in the robustness measurement.

The experiments of $\mathcal{R}(g, D_s^7, d_{S1}(M=10,000))$ and $\mathcal{R}(g, D_s^7, d_{S2}(r_0=1.0))$ are conducted to measure the changing value of g due to the extra 10,000 trips per hour and twice a station’s stable travel demand per hour in the morning peak hour (7:00 a.m.–8:00 a.m.). The results are shown in Fig. 5 (a) and (b) and they both pinpoint some key stations that are sensitive to extra travel demand with higher capacity loss (the highest adaptability value of 0.38). Next, the experiments of $\mathcal{R}(g, D_s^7, d_{S3}(r_1=0-0.1))$ are conducted to measure the changing value of g due to an increase ratio ($r_1 \in [0.00, 0.10]$) of all the stations’ travel demand in the same time frame. Different from the result in Fig. 4 (c) that the robustness improves with the increase of α , Fig. 5 (c) shows that with $\alpha \leq 0.3$, the adaptability is the best as the changing value is 0; with $\alpha = 0.4$, the adaptability is the worst as the changing value is the largest; and after increasing α from 0.4 to 0.7, the adaptability gets better as the changing value becomes smaller. The results show that either a small increase in the capacity of other types of transport networks or a large increase in the capacity of the BSN (corresponding to a large α) can improve the adaptability of the BSN under S3. In addition, it is implied that the same level of increase in the network capacity may have different effects on robustness and adaptability.

4.2.4. Recoverability

Recoverability measures the capacity of the BSN to recover from a disruption during a time frame. The experiments of $\mathcal{R}(g, D_s^k, d_{S1}(M=10,000))$, $\mathcal{R}(g, D_s^k, d_{S2}(r_0=1.0))$, and $\mathcal{R}(g, D_s^k, d_{S3}(r_1=0.1))$, $k \in [5, 23]$ are conducted to measure how much pressure the network is faced under different travel demands in different timeslots. Under S1 and S2, the Pinguoyuan Station in Fig. 6 (f), the most sensitive station to extra travel demand in Figs. 4 and 5, is selected as a representative. Fig. 6 (a) shows the different recovery triangles formed by the areas between the curve of $g = 1$ and other g curves associated with different α . The recovery triangles are basically composed of two series: morning (5:00 a.m.–10:00 a.m.) and evening (16:00 p.m.–20:00 p.m.) triangles. The areas of morning triangles on average are much larger than their counterpart. The sum of the areas of the two triangles is taken as the recoverability. Fig. 6 (b), (c), and (d) show the different effects that the demand

disruptions have on the BSN. The recoverability shows a similar decreasing trend to Fig. 6 (a) and the areas of the latter three are all larger than that of the former one. Fig. 6 (e) shows the relationships between the recoverability and α of the former four subfigures. They all fit well with exponential decay distributions: under $d = 0$, $R_3 = 4.31 * e^{-5.59\alpha}$ with $R^2 = 0.99$; under $d = S1$, $R_3 = 5.18 * e^{-3.65\alpha}$ with $R^2 = 0.96$; under $d = S2$, $R_3 = 4.65 * e^{-4.79\alpha}$ with $R^2 = 0.99$; and under $d = S3$, $R_3 = 5.85 * e^{-4.56\alpha}$ with $R^2 = 0.98$. When $\alpha = 0$, the recoverability of the four scenarios reaches the highest values of 4.35, 5.00, 4.58, and 5.58, meaning the worst recoverability at this point.

According to Fig. 6, the following conclusions can be drawn. First, the network suffers from much traffic pressure and capacity shortage in the morning and evening peak hours, and the shortage in the morning peak is much larger. This indicates that D_s has a great impact on the BSN’s recoverability and it is in an urgent state to control the travel demand in peak hours. Second, with the increase of α , the network performance gets better and the effects get weaker after 0.4. This indicates that to economically improve the network performance, the dynamic increase in capacity shall be applied according to the different congestion levels of the BSN sections. Third, in Fig. 6 (e), the areas under S1 and S3 are always larger than those under S2 and the normal state, and after $\alpha = 0.1$ the areas under S1 are larger than those under S3. This indicates that a small amount of extra travel demand on one key station (around 10,000 trips per hour) can do greater harm to the BSN than a large amount of extra travel demand on the network (around 60,000 trips per hour). The results again confirm the importance of pinpointing the key stations for travel demand management and control.

5. Remarks and policy implications

From all the measurement results in the three dimensions of the BSN, we make the following remarks. First, FR reflects the dynamic network performance as the FR dimensions are all dynamic over time responding to the spread of disruption and the propagation of traffic flows. Second, using the FR measurement framework, the time-varying bottleneck nodes and edges can be pinpointed precisely, which is important for guiding traffic control and management. Third, the same level of increase in the network capacity may result in different levels of improvement in robustness and adaptability, implying that it is crucial

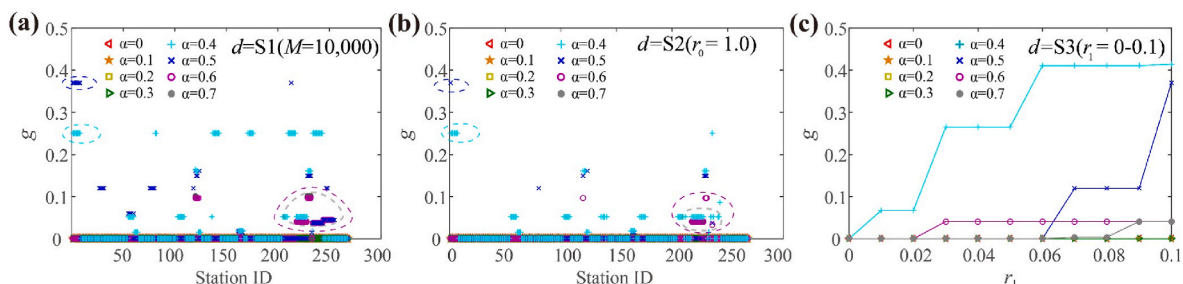


Fig. 5. The adaptability of the BSN under S1, S2, and S3.

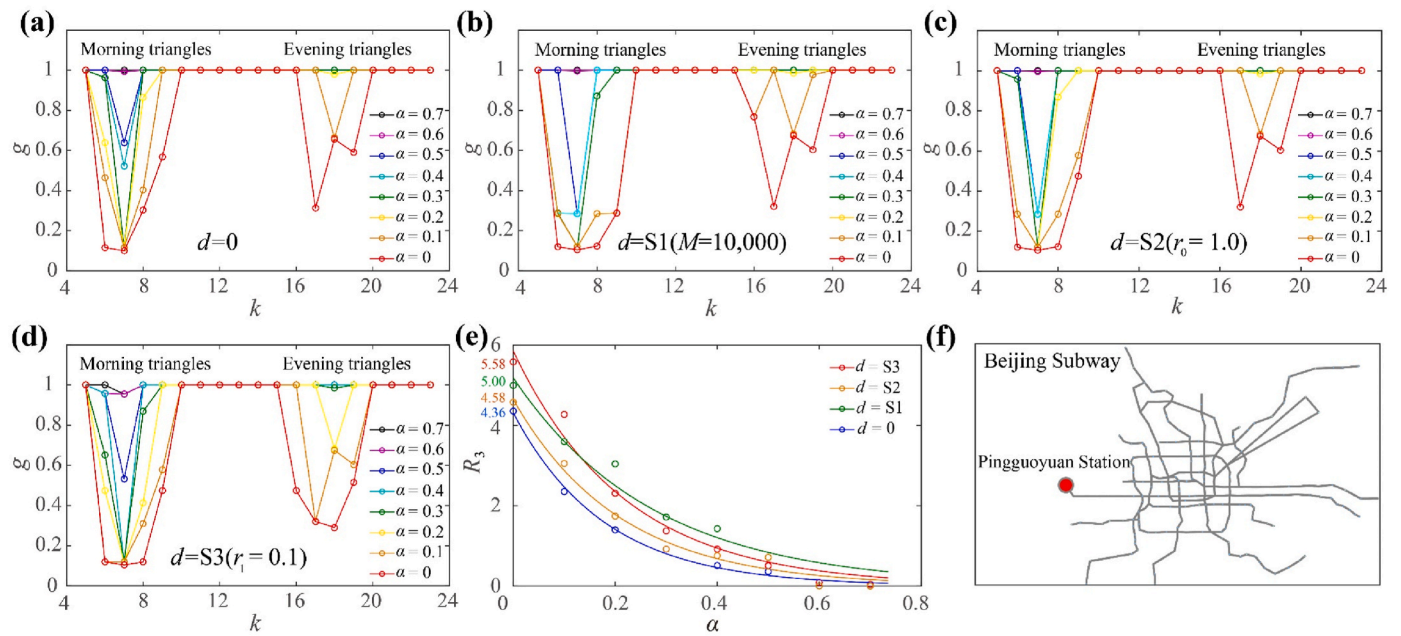


Fig. 6. The recoverability of the BSN under S1, S2, and S3.

to interlink the capacity expansion plans with the different dimensions of resilience.

With the case study, the detailed policy suggestions to improve the FR are made based on the analysis of the FR dimensions according to the order of recoverability, robustness, and adaptability. The explanations are as follows. First, it is important to find out what the key time frames are. From the recoverability results in Fig. 6, the BSN suffers from the largest capacity loss in the morning hours (5:00 a.m.–10:00 a.m.) and evening hours (16:00 p.m.–20:00 p.m.). These two time frames should receive more attention. The next is to identify where the key bottlenecks are. Based on the robustness results in Fig. 4, some representative stations sensitive to S1 and S2 are pinpointed by the dashed ovals, e.g., the Pingguoyuan, Tiantongyuan, Xierqi, Huilongguan, and Huoying stations, which have the highest travel demands in reality. Thereafter, control policies can be devised accordingly. From the demand side, the operators may perform travel demand management at the key stations surrounded by different dashed ovals in Figs. 4 and 5 in morning peak hours because a key station’s surging travel demand can result in capacity reduction as high as 38% of the entire network. For example, the policies include controlling travel demand and guiding passengers to less congested travel options. From the supply side, the BSN operator can improve the FR by dynamically adjusting the capacities of the lines or deploying extra shuttle bus services on the lines connecting to the bottlenecks under scenarios S1 and S2. Also, it is suggested to only increase the capacity of other types of transport networks slightly to deal with S3 as it needs a huge capacity increase in itself for a small amount of extra travel demand. Finally, we compare the improvement trends of adaptability and robustness under different policies. Taking S3 in Figs. 4 and 5 for example, it can be observed that when the capacity increment ratio (the overload tolerance parameter) is larger than 0.5, the improvement trends and effects of robustness and adaptability are the same. Based on these three sequential analyses, the improvement policies are more relevant for the BSN.

6. Conclusions and future work

This study proposes an application-oriented framework for measuring FR. It can measure the dynamic FR of transport networks without external interventions under supply and demand disruptions. We compile three capacity-related dimensions from the literature,

including robustness (capacity surplus), adaptability (capacity change), and recoverability (cumulative capacity loss) in a single framework. For application purposes, we summarize the necessary components for a resilience measurement model. In the case study of the BSN, the results show the framework’s advantages in grasping the dynamics of network performance, pinpointing the time-varying network bottlenecks, and assessing the influence of the dynamic capacity expansion. The operators may use the recoverability to predict when to focus, the robustness to pinpoint where to concern, and the adaptability to finally ensure how to make the specific control measures.

Despite the comprehensiveness of the proposed measurement framework, there are several limitations worth further investigation. First, a few single-layer networks complement and compete with each other (Zheng et al., 2018), it would be interesting to measure to what extent and in which particular dimensions the multi-layer networks (e.g., Liao et al., 2013, 2014; Jiang et al., 2021) improve FR. Second, the measured FR results at the new equilibrium state may overestimate the transient FR performance since during the timeslot, there may exist a time point when the transient FR is worse than that at the new equilibrium. While the proposed formulation can deliver the transient FR performance, the challenge of interpreting the results arises and thus it is important to select other meaningful reference points. Third, in the operationalization, the classic four-step model is applied, which has been criticized for the validity of modeling interdependencies. Since the proposed measurement framework is generic, it is feasible to incorporate more realistic travel behavior modeling mechanisms (He and Liu, 2012; Nogal et al., 2016; Wang et al., 2019). Fourth, the “dynamics” can be reflected by the real dynamic travel demands, dynamic transport supplies, and the continuous effects of travel flows between neighboring time frames. In the case study, we endeavor to identify the time-varying bottlenecks with relatively low time resolutions (1 h). As dynamic traffic assignment in a high time resolution is time-costly in large-scale transport networks, the dynamics are not fully explored. We will address these issues in our future work.

Author statement

Junjie Wang: Conceptualization; Methodology; Writing – Original Draft; Data collection and analysis.

Feixiong Liao: Conceptualization; Methodology; Writing – Review

& Editing; Supervision.

Jianjun Wu: Data provision; Conceptualization; Supervision.

Huijun Sun: Data analysis; Review.

Weiping Wang: Conceptualization; Methodology; Review.

Ziyou Gao: Writing – Review & Editing; Supervision.

Data and codes availability statement

The data can be accessed through an agreement with the Beijing metro company and the codes that support the findings of this study are available at the link <https://figshare.com/s/c29a6d573d2aacd96775>.

Declaration of competing interest

The authors declare that they have no known competing financial

interests or personal relationships that could have appeared to influence the work reported in this paper.

Data availability

The authors do not have permission to share data.

Acknowledgements

This work is jointly supported by the National Natural Science Foundation of China (72288101, 72101018, 71890972/71890970, 72271127, 72001023) and the Dutch Research Council (NWO). The first author is grateful to the financial support by the China Scholarship Council (202007090090).

Appendix 1. Tables

Table A1

Primary notations

| Parameters | Definitions |
|--|--|
| $C_E(u), C_{E_1}(u), C_{E_2}(u)$ | the carrying capacities of edge u of different transport networks |
| $C_V(i)$ | the carrying capacity of node i |
| d_{SS} | supply side failure |
| D^k | the total travel demand in the k -th timeslot |
| D_c^k | the extra travel demand in the k -th timeslot |
| D_s^k | the stable travel demand in the k -th timeslot |
| $D^k(i, j)$ | the total travel demand from node i to node j in the k -th timeslot |
| $D_c^k(i, j)$ | the extra travel demand from node i to node j in the k -th timeslot |
| $D_s^k(i, j)$ | the stable travel demand from node i to node j in the k -th timeslot |
| $F(I)$ | the traffic flow in the I -th iteration |
| g | the ratio of the maximum connecting subgraph |
| G_m | the maximum connecting subgraph of the network G |
| $G(V, E)$ | the transportation network composed of node set V and edge set E |
| K | the entire time frame is divided into K timeslots, $K \in N^+$ |
| n_c | the number of train carriages |
| n_G, n_{G_m} | the number of edges or nodes in G and G_m |
| $q_E(u), q_{E_1}(u), q_{E_2}(u)$ | the traffic volume on edge u of different transport networks |
| $q_V(i)$ | the traffic volume through node i |
| r_0, r_1 | travel demand increasing ratio on each node and the entire network |
| r_{SS} | supply side failure ratio of the network |
| R_1, R_2, R_3 | three resilience dimensions of robustness, adaptability, and recoverability |
| $\mathcal{R}(x, D_s^k, d, t)$ | a general measurement formula of network resilience |
| $t_1(u), t_0(u)$ | the actual or perceived travel time and free flow travel time of edge u , respectively |
| t_h | the headway of a subway line |
| t_b^k, t_w^k, t_f^k | the beginning, worst, and finishing time of a disrupted timeslot k , respectively |
| $\hat{t}(i, j), t(i, j)$ | the travel time between node i and node j with and without d and D_s^k |
| T', T | the sums of the inverse travel time with and without d and D_s^k |
| $Y(I)$ | the augmented traffic flow in the I -th iteration |
| α | the overload parameter |
| $\beta_1, \theta_1, \beta_2, \theta_2$ | two pairs of calibrated parameters in the BPR equation |
| ρ | the scaling coefficient of the capacity |
| λ | the rated carrying capacity per carriage |

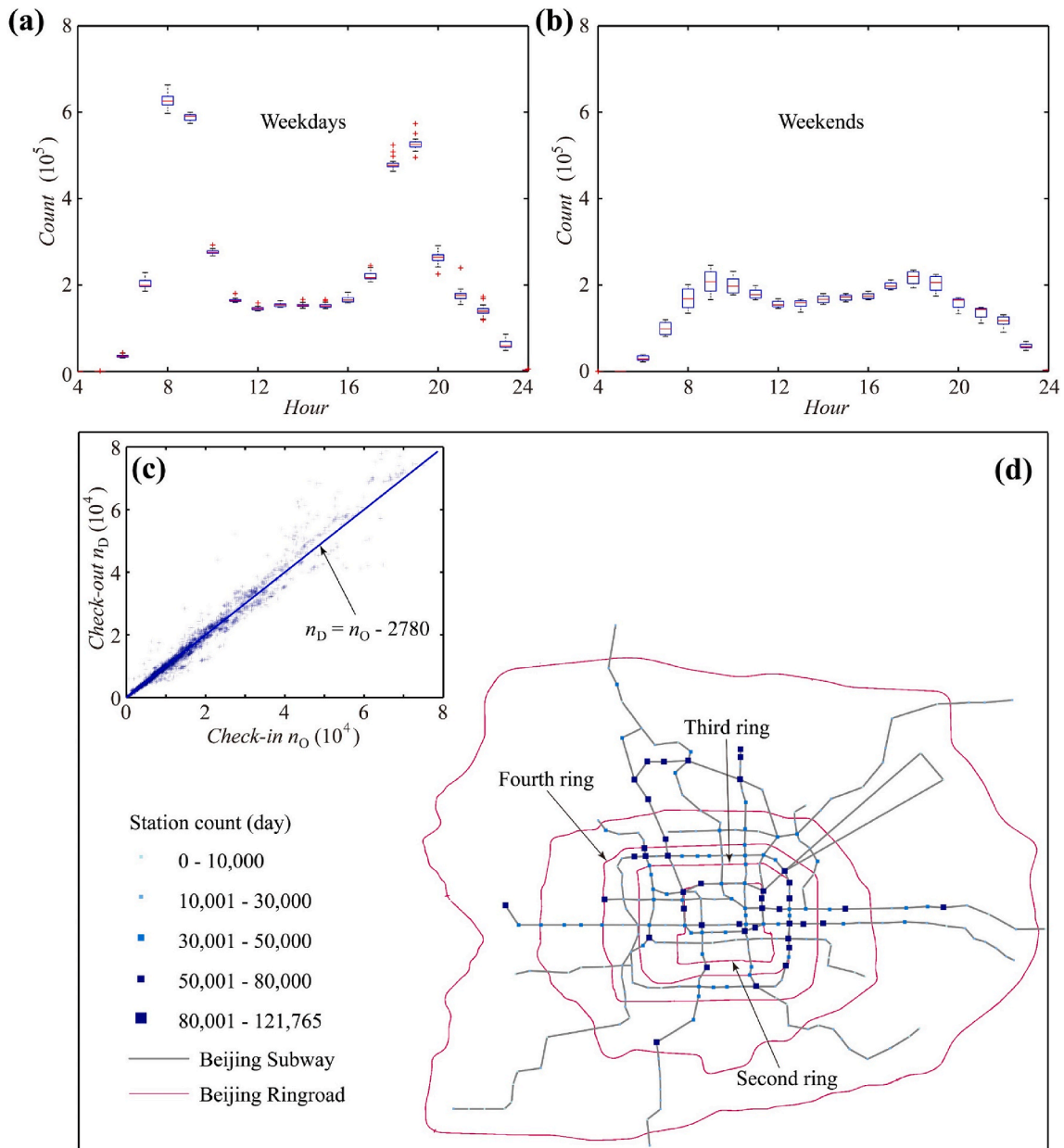


Fig. A1. Regularity and volatility of travel demand on the BSN.

displays the daily numbers of check-in and check-out passengers at each station. For each station, the numbers of daily check-in and check-out passengers are almost the same and show a linear pattern with an R-squared value $R^2 = 0.9756$, which also indicates the stability of the travel demand. Fig. A1 (d) shows the uneven spatial distribution of daily station-based travel demand. It is seen that stations with higher travel demand are mainly distributed near the second, third, and fourth rings in the east and north. Based on these plots, we can see that the stability and volatility of the travel demands co-exist. In line with Eqs. (6) and (7), travel demand can be divided into two parts, i.e., stable travel demand (D_s) and extra travel demand (D_e).

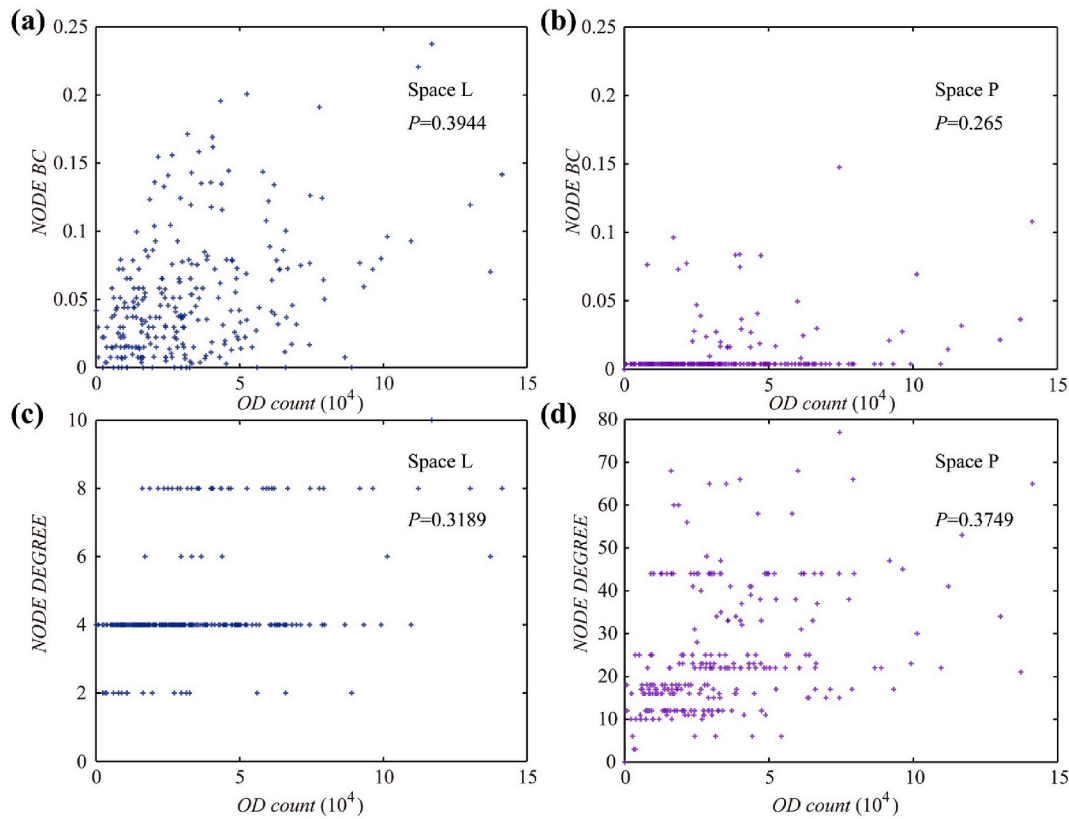


Fig. A2. Low correlation between structural indices and travel demand of the BSN.

To investigate the network importance reflected by the real travel demand and network structure, we apply the Space P and L methods (Sienkiewicz and Holyst, 2005) to rebuild the BSN. The Space P method considers a subway line as a strongly connected graph and the interchange station as the connection between different lines to construct an interchange network, while the Space L method considers each station as a node and the sections between two neighboring stations as the edges to construct a spatial network. Each node degree (the sum of in-degree and out-degree) and each node betweenness centrality (BC) are calculated to compare with the real node travel demand. Fig. A2 (a) to (d) depict the daily OD count versus node BC using Space L, OD count versus node BC using Space P, OD count versus node degree using Space L, and OD count versus node degree using Space P, respectively. The Pearson correlation coefficients (P) between structural indices (node degree and BC) and the average number of OD pairs per day at each station are comparatively low and under 0.4. Especially, some edges with high traffic flows may be insignificant structurally. Wang et al. (2013) also observed the low correlations between structural indices and real traffic demand. Therefore, the neglect of traffic demand distribution on the network tends to cause false identification of important nodes or edges opposed to the reality. Thus, SR derived from structural indices is insufficient to reveal the resilience of a transportation network during a short time frame.

The preliminary analyses of the datasets indicate that the topological importance and the real travel demand of a transport network are not strongly related, and this is the major motivation for studying the FR of a transport network.

Appendix 3. The recoverability using the index of mean harmonic distance

Another new connectivity index (Wang et al., 2018; Ganin et al., 2019) is used to measure the recoverability dimension of the BSN and the results are presented below.

This index represents the “mean harmonic distance” of a network and can be calculated by the sum of “inverse travel time” between all pairs of nodes:

$$T' / T = \frac{\sum_{i,j \in V, i \neq j} \frac{1}{t(i,j)}}{\sum_{i,j \in V, i \neq j} \frac{1}{t(i,j)}} \tag{A1}$$

where T' and T are the sums of the inverse travel time between any pair of nodes without and with d and D_s^k ; $t(i,j)$ and $t(i,j)$ are the travel times between nodes i and j with and without d and D_s^k , respectively; V is the surviving node set after disruptions. Through the comparison between T and T' , it translates the efficiency-related index (T) to a “capacity surplus” index (T'/T). Similarly, it can be transformed to the “capacity change” and “cumulative capacity loss” indices. It can better reflect all the surviving network components than g .

Fig. A3 (b), (c), and (d) show the different effects that the demand disruptions have on the BSN. The recoverability shows a similar decreasing trend to Fig. A3 (a) with the increase of α and the areas of the latter three are all larger than that of the former one. It depicts the negative influence of the extra travel demand on the network. Fig. A3 (e) shows the relationships between the recoverability and overload parameter α of the former four subfigures. They all fit well with exponential decay distributions: under $d = 0$, $R_3 = 5.15 * e^{-5.53\alpha}$ with $R^2 = 0.99$; under $d = S1$, $R_3 = 6.19 * e^{-3.66\alpha}$

with $R^2 = 0.96$; under $d = S2$, $R_3 = 5.54 * e^{-4.82\alpha}$ with $R^2 = 0.98$; and under $d = S3$, $R_3 = 6.26 * e^{-4.24\alpha}$ with $R^2 = 0.97$. When $\alpha = 0$, the worst recoverability of the four scenarios are 5.19, 5.42, 5.92, and 5.92.

In comparison of Fig. 6 with Fig. A3, except that T^i/T shows larger negative effects than g , we can obtain almost the same results using the two different indices. It is because a targeted index's results before and after disruptions can always be normalized by defining the smaller values as the numerator and the larger ones as the denominator (Ganin et al., 2019). Therefore, all the indices can be capsulated into x , and the framework becomes more convenient and comprehensive.

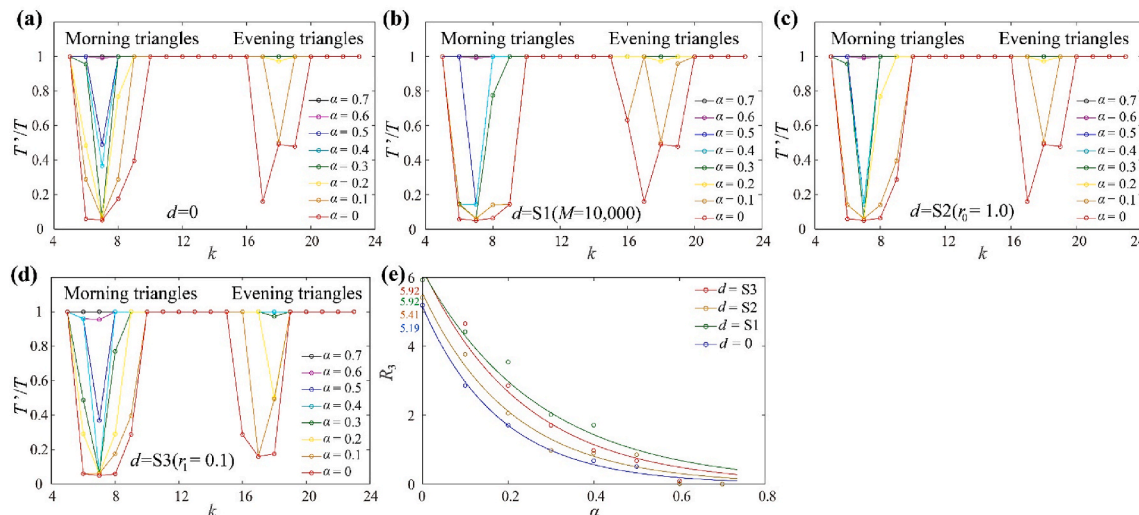


Fig. A3. The recoverability of the BSN under S1, S2, and S3 using mean harmonic distance.

References

Baroud, H., Barker, K., Ramirez-Marquez, J.E., Claudio, M.R.S., 2014. Importance measures for inland waterway network resilience. *Transport. Res. Part E* 62, 55–67.

Berdica, K., 2002. An introduction to road vulnerability: what has been done, is done and should be done. *Transport Pol.* 9, 117–127.

Bruneau, M., Chang, S.E., Eguchi, R.T., Lee, G.C., O'Rourke, T.D., Reinhorn, A.M., Shinozuka, M., Tierney, K., Wallace, W.A., Von Winterfeldt, D., 2003. A framework to quantitatively assess and enhance seismic resilience of communities. *Earthq. Spectra* 19 (4), 733–752.

Bureau of Public Roads, 1964. *Traffic Assignment Manual*. U.S. Department of Commerce, Urban Planning Division, Washington, DC.

Cats, O., Jenelius, E., 2015. Planning for the unexpected: the value of reserve capacity for public transport network robustness. *Transport. Res. Part A* 81, 47–61.

Chen, L., Miller-Hooks, E., 2012. Resilience: an indicator of recoverability in intermodal freight transport. *Transport. Sci.* 46 (1), 109–123.

Cohen, R., Erez, K., Ben-Avraham, D., Havlin, S., 2000. Resilience of the internet to random breakdowns. *Phys. Rev. Lett.* 85 (21), 4626–4628.

Cox, A., Prager, F., Rose, A., 2011. Transportation security and the role of resilience: a foundation for operational metrics. *Transport Pol.* 18, 307–317.

Espinete, X., Schweikert, A., Nicola, V.D.H., Chinowsky, P., 2016. Planning resilient roads for the future environment and climate change: quantifying the vulnerability of the primary transport infrastructure system in Mexico. *Transport Pol.* 50, 78–86.

Galaitis, S., Keisler, J., Trump, B., Linkov, I., 2020. The need to reconcile concepts that characterize systems facing threats. *Risk Anal.* 41 (1), 3–15.

Galaitis, S., Kurth, M., Linkov, I., 2021. Resilience: direction for an uncertain future following the COVID-19 pandemic. *Geohealth* 5 (11).

Ganin, A., Kitsak, M., Marchese, D., Keisler, J.M., Seager, T., Linkov, I., 2017. Resilience and efficiency in transportation networks. *Sci. Adv.* 3 (12), e1701079.

Ganin, A., Mersky, A., Jin, A., Kitsak, M., Keisler, J., Linkov, I., 2019. Resilience in intelligent transportation systems (ITS). *Transport. Res. C Emerg. Technol.* 100, 318–329.

Gu, Y., Fu, X., Liu, Z., Xu, X., Chen, A., 2020. Performance of transportation network under perturbations: reliability, vulnerability, and resilience. *Transport. Res. Part E* 133, 101809, 1–16.

He, X., Liu, H.X., 2012. Modeling the day-to-day traffic evolution process after an unexpected network disruption. *Transport. Res. Part B* 46 (1), 50–71.

Henry, D., Ramirez-Marquez, J.E., 2012. Generic metrics and quantitative approaches for system resilience as a function of time. *Reliab. Eng. Syst. Saf.* 99, 114–122.

Holme, P., Kim, B.J., Yoon, C.N., Han, S.K., 2002. Attack vulnerability of complex networks. *Phys. Rev.* 65 (5), 056109.

Hosseini, S., Barker, K., Ramirez-Marquez, J.E., 2016. A review of definitions and measures of system resilience. *Reliab. Eng. Syst. Saf.* 145, 47–61.

Jiang, Y., Liao, F., Jin, L., 2021. Effects of locational accessibility on firm diffusion characteristics: the case of Sino-Europe Economic Corridor. *Transport Pol.* 105, 80–93.

Kermanshah, A., Derrible, S., 2017. Robustness of road systems to extreme flooding: using elements of GIS, travel demand, and network science. *Nat. Hazards* 86, 151–164.

Kitsak, M., Ganin, A., Eisenberg, D., Krapivsky, P., Krioukov, D., Alderson, D., Linkov, I., 2018. Stability of a giant connected component in a complex network. *Phys. Rev. E* 97 (1), 012309.

Li, C., Fang, Q., Ding, L., Cho, Y.K., Chen, K., 2020. Time-dependent resilience analysis of a road network in an extreme environment. *Transport. Res. Part D* 85, 102395.

Liao, F., van Wee, B., 2017. Accessibility measures for robustness of the transport system. *Transportation* 44, 1213–1233.

Liao, F., Arentze, T., Timmermans, H., 2013. Incorporating space-time constraints and activity-travel time profiles in a multi-state supernetwork approach to individual activity-travel scheduling. *Transport. Res. Part B* 55, 41–58.

Liao, F., Arentze, T., Timmermans, H., 2014. Multi-state supernetworks: recent progress and prospects. *J. Traffic Transport. Eng.* 1 (1), 13–27.

Linkov, I., Bridges, T., Creutzig, F., Decker, J., Fox-Lent, C., Kröger, W., Lambert, J.H., Levermann, A., Montreuil, B., Nathwani, J., Nyer, R., Renn, O., Scharte, B., Scheffler, A., Schreurs, M., Thiel-Clemen, T., 2015. Changing the resilience paradigm. *Nat. Clim. Change* 4 (6), 407–409.

Liu, P., Liao, F., Huang, H.-J., Timmermans, H., 2016. Dynamic activity-travel assignment in multi-state supernetworks under transport and location capacity constraints. *Transportmetrica: Transport. Sci.* 12 (7), 572–590.

Motter, A.E., Lai, Y.C., 2002. Cascade-based attacks on complex networks. *Phys. Rev.* 66 (6), 065102.

Murray-Tuite, P.M., 2006. A comparison of transportation network resilience under simulated system optimum and user equilibrium conditions. In: *Proceedings of the 2006 Winter Simulation Conference*, pp. 1398–1405.

Nogal, M., Honfi, D., 2019. Assessment of road traffic resilience assuming stochastic user behaviour. *Reliab. Eng. Syst. Saf.* 185, 72–83.

Nogal, M., O'Connor, A., Caulfield, B., Martinez-Pastor, B., 2016. Resilience of traffic networks-From perturbation to recovery via a dynamic restricted equilibrium model. *Reliab. Eng. Syst. Saf.* 156, 84–96.

Pimm, S.L., 1984. The complexity and stability of ecosystems. *Nature* 307, 321–326.

Poon, M., Wong, S., Tong, C., 2004. A dynamic schedule-based model for congested transit networks. *Transport. Res. Part B* 38 (4), 343–368.

Qin, J., Liao, F., 2021. Space-time prism in multimodal supernetwork-Part 1: Methodology. *Communications in Transportation Research* 1, 100016.

Reggiani, A., Nijkamp, P., Lanzi, D., 2015. Transport resilience and vulnerability: the role of connectivity. *Transport. Res. Part A* 81, 4–15.

Serdar, M.Z., Koç, M., Al-Ghamdi, S.G., 2022. Urban transportation networks resilience: indicators, disturbances, and assessment methods. *Sustain. Cities Soc.* 76 (2022), 103452.

Sienkiewicz, J., Holyst, J.A., 2005. Statistical analysis of 22 public transport networks in Poland. *Phys. Rev.* 72, 046127.

UIC, 2004. *Capacity (UIC Code 406)*. International Union of Railways (UIC), Paris, France.

- Wang, J., Li, Y., He, K., Wang, P., 2013. Vulnerability analysis and passenger source prediction in urban rail transit networks. *PLoS One* 8 (11), e80178.
- Wang, W., Yang, S., Hu, F., Stanley, H.E., He, S., Shi, M., 2018. An approach for cascading effects within critical infrastructure systems. *Phys. Stat. Mech. Appl.* 510, 164–177.
- Wang, D., Liao, F., Gao, Z., Timmermans, H., 2019. Tolerance-based strategies for extending the column generation algorithm to the bounded rational dynamic user equilibrium problem. *Transport. Res. Part B* 119, 102–121.
- Wang, W., Yang, S., Stanley, H.E., Gao, J., 2019. Local floods induce large-scale abrupt failures of road networks. *Nat. Commun.* 10 (1), 1–11.
- Wardrop, J.G., 1952. Road paper. some theoretical aspects of road traffic research. *Proc. Inst. Civ. Eng.* 1 (3), 325–362.
- Wu, J., Li, D., Si, S., Gao, Z., 2021. Special issue: reliability management of complex system. *Frontiers of Engineering Management* 8 (4), 477–479.
- Yosef, K., Gilad, B., Yaakov, T., Benjamin, K., Gabriel, C., Buldyrev, S.V., 2018. Network overload due to massive attacks. *Phys. Rev.* 97 (52309), 1–10.
- Zeng, G., Li, D., Guo, S., Gao, L., Gao, Z., Stanley, H.E., Havlin, S., 2019. Switch between critical percolation modes in city traffic dynamics. *Proc. Natl. Acad. Sci. U.S.A.* 116 (1), 23–28.
- Zeng, G., Sun, Z., Liu, S., Chen, X., Li, D., Wu, J., Gao, Z., 2021. Percolation-based health management of complex traffic systems. *Frontiers of Engineering Management* 8 (4), 557–571.
- Zhang, X., Miller-Hooks, E., Denny, K., 2015. Assessing the role of network topology in transportation network resilience. *J. Transport Geogr.* 46, 35–45.
- Zhang, L., Zeng, G., Li, D., Huang, H., Stanley, H.E., Havlin, S., 2019. Scale-free resilience of real traffic jams. *Proc. Natl. Acad. Sci. U.S.A.* 116 (18), 8673–8678.
- Zheng, Z., Huang, Z., Zhang, F., Wang, P., 2018. Understanding coupling dynamics of public transportation networks. *EPJ Data Science* 7 (23), 1–16.
- Zhou, Y., Wang, J., Yang, H., 2019. Resilience of transportation systems: concepts and comprehensive review. *IEEE Trans. Intell. Transport. Syst.* 20 (12), 4262–4276.
- Zuo, M., 2021. System reliability and system resilience. *Frontiers of Engineering Management* 8 (4), 615–619.